Clays and Clay Minerals, Vol. 48, No. 3, 374–384, 2000.

TRANSMISSION ELECTRON MICROSCOPY STUDY OF ILLITIZATION IN PELITES FROM THE IBERIAN RANGE, SPAIN: LAYER-BY-LAYER REPLACEMENT?

BLANCA BAULUZ,[1] DONALD R. PEACOR,[2] AND JOSE MANUEL GONZALEZ LOPEZ[1]

[1]Departamento de Ciencias de la Tierra, Cristalografia y Mineralogia, Universidad de Zaragoza, 50.009 Zaragoza, Spain
[2]Department of Geological Sciences, The University of Michigan, Ann Arbor, Michigan 48109-1063, USA

Abstract—A sequence of interstratified illite-smectite (I-S) and illite in Paleozoic pelites and metapelites from the Iberian Range, Spain, was studied by X-ray diffraction (XRD), scanning electron microscopy (SEM), and transmission electron microscopy (TEM). The fine-grained matrix of diagenetic pelites is composed of I-S with sequences of illite- and smectite-like layers in a given sample. The Reichweite (R) values as determined by XRD and averaged over heterogenous I-S layer sequences increase with increasing grade, apparently continuously, in sharp contrast with TEM observations of other published sequences. Changes in I-S sequences along layers are rarely observed. In the higher-grade diagenetic pelites, I-S coexists with illite. Each I-S phase has a composition similar to that of illite, implying unique Al-Si distributions in contrast to smectite and muscovite. Selected area electron diffraction (SAED) patterns of I-S and illite are diagnostic of $1M_d$ polytypism. Anchizonal metapelites consist of larger packets of well-crystallized muscovite, with SAED patterns corresponding to a two-layer polytype.

The continuous sequence of changes studied by TEM in I-S sequences and lateral transitions among these units is consistent with illitization by layer-by-layer replacement, although other processes are possible also. Replacement of individual layers probably occurs via fluids at reaction interfaces, in contrast to solid-state reactions, *sensu strictu*. The transition from the diagenetic to anchizonal rocks (transition in textures and formation of muscovite-$2M_1$) occurred via dissolution/crystallization, however, presumably by tectonic stress. XRD and TEM data imply a consistent prograde trend in the sequence, the XRD data defining the average, long-range Reichweite ordering sequence, whereas the TEM data define the short-range layer sequences.

Key Words—Analytical Electron Microscopy, I-S, Illite, Illitization Process, Polytypism, Prograde Diagenesis, Scanning Electron Microscopy, Transmission Electron Microscopy.

INTRODUCTION

The transition from smectite to illite has been widely documented by X-ray diffraction (XRD) studies. There is general agreement, as emphasized in part by Hower *et al.* (1976), that this process involves interstratified illite-smectite (I-S) intermediates. Most studies of illitization use modeled XRD patterns of I-S to document changes in ordering of high- and low-charge layers using the Reichweite (R) notation, where R represents the number of layers affected by the presence of a given layer (Jadgozinski, 1949). Numerous studies of smectite illitization reported that smectitic I-S exhibits R = 0 ordering, illitic I-S has R = 1 ordering, and highly illitic I-S has R = 3 ordering (Hower *et al.*, 1976; Altaner *et al.*, 1984; Horton, 1985; Brusewitz, 1986). Some studies noted that (R = 2) I-S is uncommon, and where it has been described it is better explained by a mixture of R = 1 and R = 3 ordering (Środoń and Eberl, 1984).

Transmission electron microscope (TEM) studies document fine-scale changes in the sequence of illitization, including increasing perfection of packets of layers, in part reflected in the increased thickness of layer sequences within which there is coherency. Coherency is indicated by the presence of 4.5-Å cross fringes that extend across 10-Å fringes in TEM images and by polytypic sequences (Lee *et al.*, 1985; Ahn and Peacor, 1986; Buatier *et al.*, 1992; Freed and Peacor, 1992; Dong and Peacor, 1996). Several TEM studies indicated that (R = 1) I-S (>50% illite) is relatively abundant, whereas other interstratified I-S sequences (*i.e.*, R > 1) are rarely observed (Ahn and Peacor, 1989; Veblen *et al.*, 1990; Jiang *et al.*, 1990; Dong and Peacor, 1996; Dong *et al.*, 1997). Dong *et al.* (1997) studied smectitic and illitic clays from different occurrences and lithologies (shales from the Gulf Coast; Nankai Trough, Japan; the Michigan Basin; the Welsh sedimentary basin; and hydrothermally altered bentonite from Zempleni, Hungary). All samples show mostly different proportions of discrete layer sequences of smectite, (R = 1) I-S or illite, where the illite occurs in 10-Å layer sequences with few (<15%) or no smectite-like layers. Other interstratified sequences with intermediate ratios of I-S were observed only as minor components representing local disorder or heterogeneity within material of dominantly (R = 1) I-S or illite. Dong *et al.* emphasized the unique Si ordering of the (R = 1) I-S structure in contrast to alternating ideal smectite and illite layers, as discussed by Nadeau *et al.* (1985) and Ahn and Peacor (1986). In (R = 1) I-S, Si ordering is symmetric across the interlayer as implied by nuclear magnetic resonance data, rather

Copyright © 2000, The Clay Minerals Society

https://doi.org/10.1346/CCMN.2000.0480308 Published online by Cambridge University Press

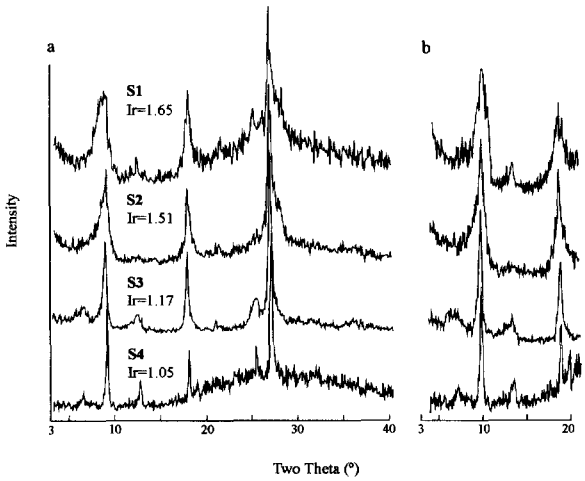


Figure 1. XRD patterns of the oriented <2-μm size fraction from the four samples selected for the TEM study. a) air-dried samples, b) ethylene glycol-solvated samples.

than across the octahedral sheet as in ideal smectite and illite (Barron *et al.,* 1985; Altaner *et al.,* 1988; Jakobsen *et al.,* 1995).

Thus, the continuous change in proportions of illite and smectite layers indicated by much XRD data is in contradiction with the discontinuous changes involving discrete smectite, (R = 1) I-S, and illite as commonly observed by TEM. Dong and Peacor (1996) argued that these differences in part were related to packet disarticulation and the averaging of heterogenous domains inherent in XRD data. However, the different conclusions regarding the nature of the interlayer sequences and transitions during illitization have been carried out on diverse sample occurrences; therefore differences in the apparent nature of the I-S sequences may be real, rather than an artifact of the method of study. It is essential, therefore, to integrate both methodologies, XRD and TEM.

The sequence of illite and smectite layers in I-S has profound consequences for the mechanism of transformation (Altaner and Ylagan, 1997, and references therein). Certainly, a discontinuous series involving discrete phases must occur via dissolution and neocrystallization in an Ostwald-step-like sequence, whereas continuous layer sequences may occur by continuous, direct replacement of individual layers. The latter might be described as a "solid-state reaction", regardless if it occurs via an essential fluid at a near-atomic scale or not (Giorgetti *et al.,* pers. comm.).

Samples appearing to represent diagenesis and low-grade metamorphism from the Iberian Range, Spain, were made available to us and previously studied by Bauluz *et al.* (1995, 1998) and Bauluz (1997). The samples were characterized by standard XRD techniques, including determinations of interstratification and polytypism, showing the presence of a continuous sequence of I-S mixed layering. We augmented the previous work with TEM data, using techniques for sample preparation (Kim *et al.,* 1995) and imaging (Guthrie and Veblen, 1989a, 1989b, 1990; Veblen *et al.,* 1990) to permit the direct identification of illite and smectite layers unaffected by sample disarticulation. We document the sequence of phases over the range of illitization to determine the mechanism of illitization as reflected in the characterized phases, and to compare the results with those obtained by XRD.

SAMPLE DESCRIPTIONS

Samples obtained were from the Iberian Range, Spain, which is comprised of Precambrian and Paleozoic sediments discordantly overlain by Permian, Triassic, and Tertiary sediments. The sediments have been affected by complex Hercynian polyphase folding and thrusting, and Alpine-age compressional events. On the basis of XRD, scanning electron microscopy (SEM), and electron microprobe (EMPA) data, Bauluz *et al.* (1995, 1998) and Bauluz (1997) concluded that Paleozoic materials are comprised of pelites and sandstones, with smaller amounts of carbonates. Clastic samples are composed of coarse detrital quartz, micas (muscovite and phengite), and minor amounts of feldspars and chlorite, whereas the fine-grained matrix is principally interstratified I-S or illite and lesser amounts of micas, chlorite, and kaolinite. XRD data showed that the samples belong to a prograde sequence ranging from diagenetic to anchizone grade. Grade was determined from XRD data of the clay fraction, including determination of polytypism and illite crystallinity (IC, Kubler, 1967; Kisch, 1991).

Four fine-grained samples were selected for TEM study from 150 samples to represent the complete range of prograde diagenesis. Samples were renumbered as S1, S2, S3, and S4, with increasing numbers corresponding to increasing grade. Samples S1, S2, and S3 have diagenetic features whereas S4 is anchizonal. Only sample S4 showed a faint rock cleavage in hand specimen, oriented subparallel to bedding. Stratigraphic data indicate that the samples were buried at depths of 3600, 4600, 6300 and 8700 m, respectively, which is consistent with the determined grade.

XRD characterization of illitic phases

XRD data were obtained using a Philips PW 1710 diffractomer, CuKα radiation, automatic divergence slit, and diffracted-beam graphite monochromator. XRD patterns of the clay fractions of samples S1, S2, and S3 have non-symmetrical 10-Å peaks (Figure 1). When samples were solvated with ethylene glycol, the 10-Å peak increased slightly in width, indicating the presence of an expandable component. According to Środoń and Eberl (1984), the position of the 002 re-

https://doi.org/10.1346/CCMN.2000.0480308 Published online by Cambridge University Press

flection in patterns of such oriented clay fractions (~17.6–17.7 °2θ) and the absence of a reflection at 32–35 °2θ suggest that the expandable component is very small and that discrete illite and a minor amount of I-S occur. The values of the parameters Ir [= the ratio of $I_{(001)}/I_{(003)}$ air-dried divided by the ratio of $I_{(001)}/I_{(003)}$ ethylene glycol treated] and BB1 and BB2 [= the joint breadth of the 001 (BB1) or 004 (BB2) illite and adjacent I-S reflections, measured in °2θ from where the tails of the peaks join the X-ray background] defined by Środoń and Eberl (1984) (BB1 and BB2 are >4 °2θ in sample S1 and <4 °2θ in samples S2 and S3) indicate that sample S1 contains illite with minor (R = 1) I-S, whereas S2 and S3 contain illite and (R = 3) I-S.

The 10-Å peak of XRD patterns of the clay fraction of sample S4 is symmetrical and does not change when treated with ethylene glycol, as consistent with the presence only of discrete illite. The IC value (Kubler, 1967; Kisch, 1991), converted to the crystallinity index standard (CIS) scale (Warr and Rice, 1994), is 0.30 °2θ. When used with the Scherrer equation, with a constant of 0.9 (Merriman *et al.,* 1990), this value is equal to a mean crystal size of 45 nm, which is consistent with anchizonal grade (Warr and Rice, 1994). The methods of Maxwell and Hower (1967) and Caillere *et al.* (1982) were used to calculate the ratio of concentrations of polytypes, $2M_1/(2M_1 + 1M + 1M_d)$. Both methods independently showed an increase in that ratio, from 0.2 to 1.0 for samples S1 through S4.

TEM PROCEDURES

The samples were treated with L.R. White resin following the procedure of Kim *et al.* (1995) to prevent collapse of smectite-like interlayers at vacuum conditions of the ion mill and TEM and to identify illite and smectite interlayers in TEM images. Great care was taken to avoid water interactions with the sample during preparation to prevent expansion of smectite and resultant sample damage. Sticky wax-backed thin sections were prepared with surfaces normal to bedding, and initially examined by optical microscopy. Representative areas were removed for SEM and TEM observations via attached Al washers, thinned in an ion mill, and carbon coated. SEM observations were made with a Hitachi S570 instrument. TEM data were obtained with a Philips CM-12 scanning-transmission electron microscope (STEM). Both the SEM and STEM were equipped with Kevex Quantum solid-state detectors and computer systems, the detector having a boron-composite window permitting analysis of low atomic-number elements. The STEM was operated at 120 kV and a beam current of 20 μA. Through-focus series of images were obtained from 1000 Å underfocus to 1000 Å overfocus, in part to obtain optimum contrast for I-S ordering (overfocus). A camera length of 770 mm and a selected-area aperture 10 μ in diameter were used to obtain selected area electron diffraction (SAED) patterns. Energy dispersive X-ray system (EDS) data were processed using Kevex software, with resultant intensity ratios being corrected with k-values determined for well-characterized samples, following the methods of Jiang and Peacor (1993). The concentration ratios were then normalized to 22 negative charges to obtain formulae.

Nomenclature for interstratification

Ordering in interstratified I-S is ordinarily characterized by its Reichweite value, on the basis of X-ray diffraction data. Such measures of I-S ordering represent long-range ordering averaged over all layers which scatter X-radiation. Short-range ordering of interlayers within I-S packets can be identified in TEM images, however. The Reichweite nomenclature is therefore inappropriate for specific layer sequences as observed by TEM. For the purpose of this study, we use the symbol I*n*, where *n* is the number of illite-like layers associated with a given smectite-like layer; *i.e.,* layers of IS are denoted as an I1 unit, ISI as an I2 unit, *etc.* This nomenclature is analogous with the Reichweite nomenclature, but applied only to specific layers. An ideal sample for which R = 1, with 50% illite-like layers, is identical to a sequence of I1 units, for example, but a sequence for which R = 1, >50% I would consist dominantly of I1 units, but also have units with $n > 1$.

SEM AND TEM RESULTS

Back-scattered electron (BSE) images of the four samples are presented in Figure 2. They show abundant detrital clasts of quartz, feldspars, micas, chlorite, and minor proportions of accessory minerals such as Ti- and Fe-oxides and apatite, all of which were identified by EDS analyses and characteristic textures. The matrices are composed of heterogeneous, fine-grained material with an average composition that is Si-, Al-, and K-rich, implying the presence of dominant dioctahedral clay minerals. The textures of samples S1, S2, and S3 (Figure 2a–2c) are those common to a relatively unmodified sediment; detrital micas are oriented subparallel to bedding, and clasts of quartz and feldspar have angular shapes, as compatible with the low grades indicated by XRD data. Sample S4 (Figure 2d) has quartz grains with rounded, fluted outlines, commonly intergrown with feldspars and micas with no detectable void space at boundaries. Such textures are caused by dissolution and crystallization of intergrown grains, and are transitional to a typical metamorphic texture, as consistent with anchizonal grade.

TEM data for samples S1, S2, and S3

TEM data were obtained primarily for the clay minerals occurring in the fine-grained matrices, assuming

https://doi.org/10.1346/CCMN.2000.0480308 Published online by Cambridge University Press

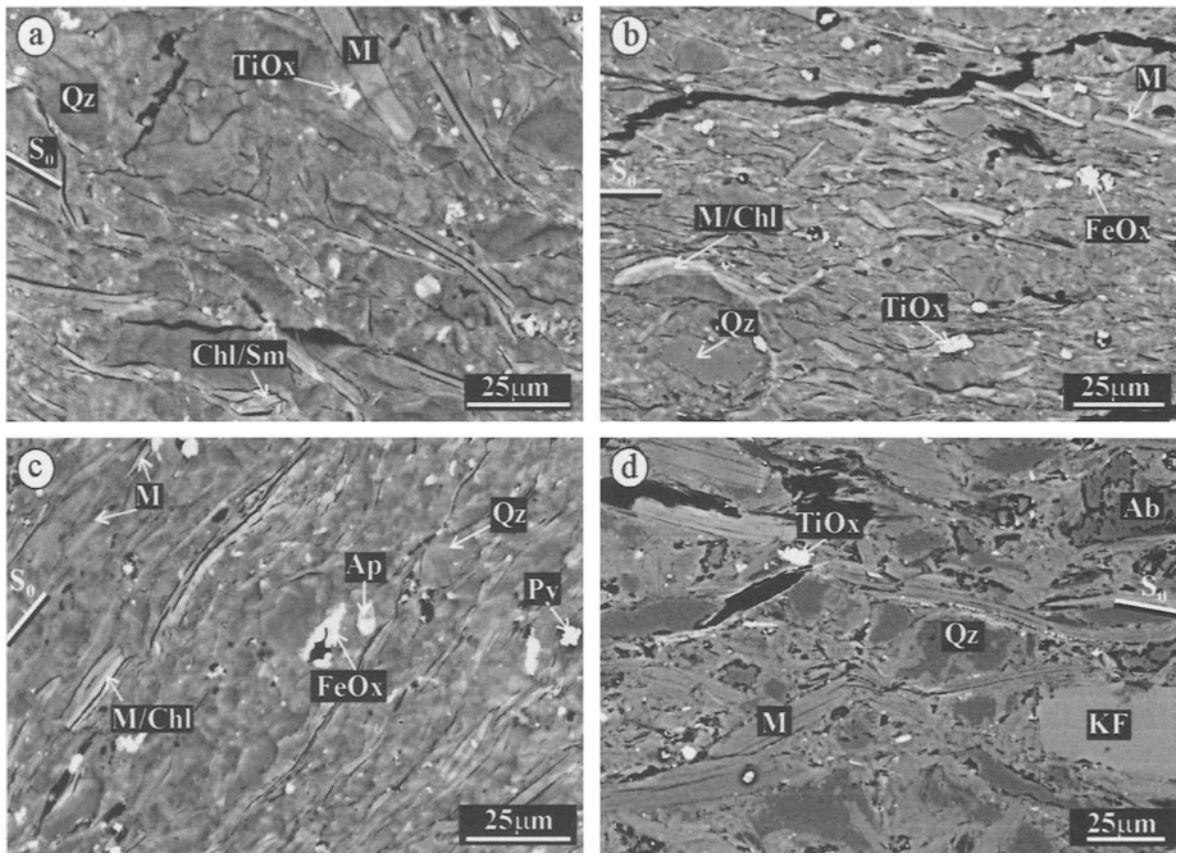


Figure 2. Back-scattered electron images of ion-milled areas of the four samples studied by TEM: a) sample S1, b) sample S2, c) sample S3, and d) sample S4. Qz = quartz, KF = K-rich feldspar, Ab = albite, M = mica, Chl/Sm = chlorite-smectite, M/Chl = mica-chlorite, FeOx = Fe-oxides, TiOx = Ti-oxides, Ap = apatite, Py = pyrite. S_0 indicates the orientation of the bedding.

that these materials dominate the clay fraction of separates used for XRD, and that such material represents authigenic clay. Lattice-fringe images of the authigenic clay minerals of samples S1, S2, and S3 are shown in Figures 3, 4, and 5, respectively. Figures 3, 4, and 5a are quite similar, the clay minerals consisting of near continuous arrays of subparallel packets of I-S, each component packet of which is ~10–20 layers thick. Fringes show alternate dark and light contrast typical of interstratified I-S (Guthrie and Veblen, 1989a, 1989b, 1990; Veblen *et al.*, 1990) with spacings related to the sums of illite and smectite layers. Thus (R = 1) I-S, with I1 units, produces images with darker and lighter fringes alternating, with d = 21–22 Å. Similarly, where fringe contrast indicated ISI or ISII layer sequences, *etc.*, measured spacings were 31–32, 41–42 Å, *etc.*, respectively. Sequences with $n \geq 7$ were observed, with the frequency generally increasing as n increased. Although a given I-value dominated a given layer sequence, other I-values occurred randomly in the same sequence. The 21–22-Å spacing of fringes having I1 periodicity, for example, is typical of I1 I-S treated with L.R. White resin, but is less than that of the sum of spacings of smectite and illite layers. Dong *et al.* (1997) noted that this result is consistent with the unique Al/Si ordering scheme and high charge of the so-called smectite-like interlayer. In addition, Figures 3 and 4 show that I-S units show fringes which are straight and with constant layer spacing, the orientations varying to a few degrees over tens of angstroms.

The TEM images were used to determine the relative proportions of the kinds of layer sequences for samples S1, S2, and S3 by counting I-units in hundreds of fringes from each sample. Some ambiguity existed in identifying illite and smectite layers owing to beam damage, but commonly because contrast is sensitive to layer orientation, sample thickness, and other factors. For example, layers without contrast may be identified as identical kinds of layers, *e.g.*, as illite, rather than as I-S, if imaging conditions are not correct and only contrast differences are used to discriminate between layer types. Layers were character-

https://doi.org/10.1346/CCMN.2000.0480308 Published online by Cambridge University Press

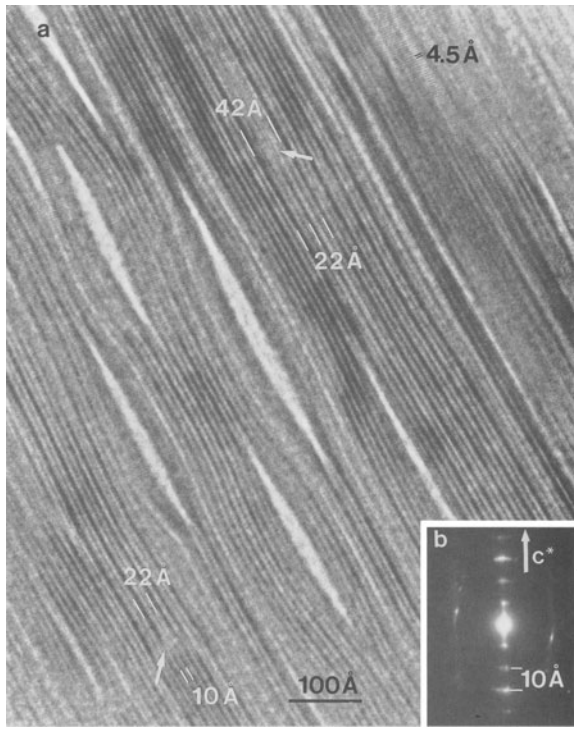


Figure 3. Lattice-fringe image (a) and SAED pattern (b) of sample S1. a) I1 I-S units with periodicity of 21–22 Å. Transitions from I1 I-S (22 Å) to illite-layers (10-Å layers) and from I1 to I3 I-S (42 Å) are shown (marked by white arrows). 4.5-Å cross-fringes are present throughout the lattice-fringe image, and are continuous across a number of 001 fringes.

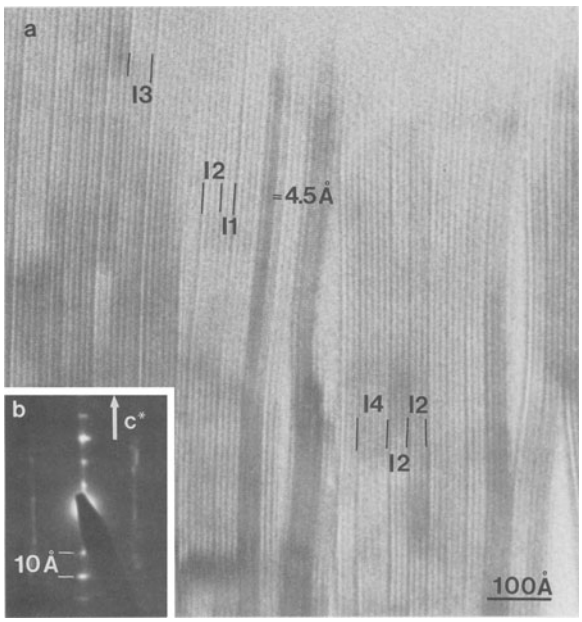


Figure 4. Lattice-fringe image (a) and SAED pattern (b) obtained using sample S2 showing a complex layer sequence with I1, I2, I3, and I4 I-S. In the area shown, the most frequent layer sequence is I2 I-S. 4.5-Å cross-fringes are present.

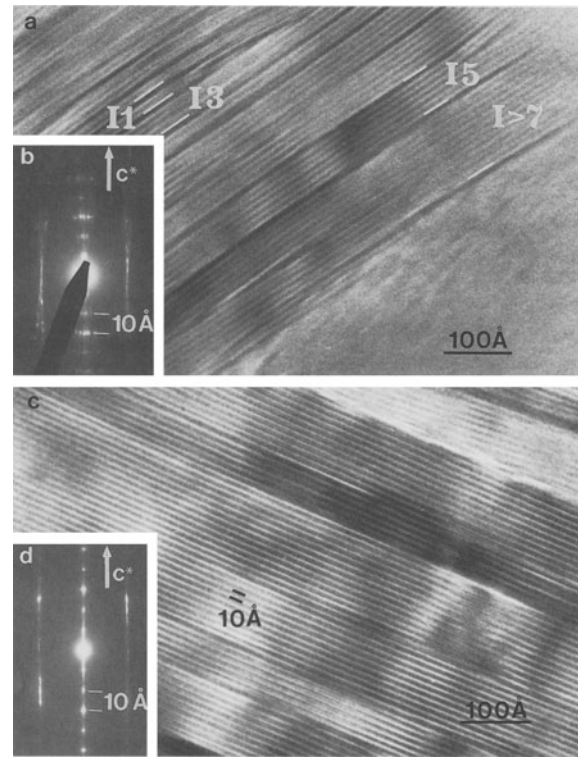


Figure 5. Lattice-fringe images (a, c) and SAED patterns (b, d) of sample S3. a) The area shown has I1 to I > 7 I-S sequences, the most frequent being I > 3 I-S. c) Illite packets with rare smectite-like layers.

ized only where both spacings and layer contrast were appropriate (Table 1).

Sequences with small proportions (<15%) of smectite-like layers were rarely observed in samples S1 and S2; they represent <10% of the clays. In sample S3, however, packets having either no or few smectite-like interlayers coexist with sequences of I-values averaging from I3 to I5 (Figure 5a and 5c). In Table 1, packets with few smectite-like interlayers, $n > 7$, are labeled as illite, although they have a small proportion of randomly interstratified smectite-like interlayers.

Illite-rich areas in sample S3 (Figure 5c) consist of packets 10–20 layers thick with sharp, well-defined boundaries. Lattice (001) fringes are straight and defect-free with constant 10-Å spacing, indicating that

Table 1. Measured numbers of units having specific I-values in each of the diagenetic samples, determined from lattice-fringe images. n = number of measurements.

		% I units						
Samples	n	I1	I2	I3	I4	I5	I6	I ≥ 7 + illite
S 1	185	41	32	8	5	5	3	6
S 2	170	19	21	18	15	13	8	6
S 3	220	7	7	7	17	10	7	45

https://doi.org/10.1346/CCMN.2000.0480308 Published online by Cambridge University Press

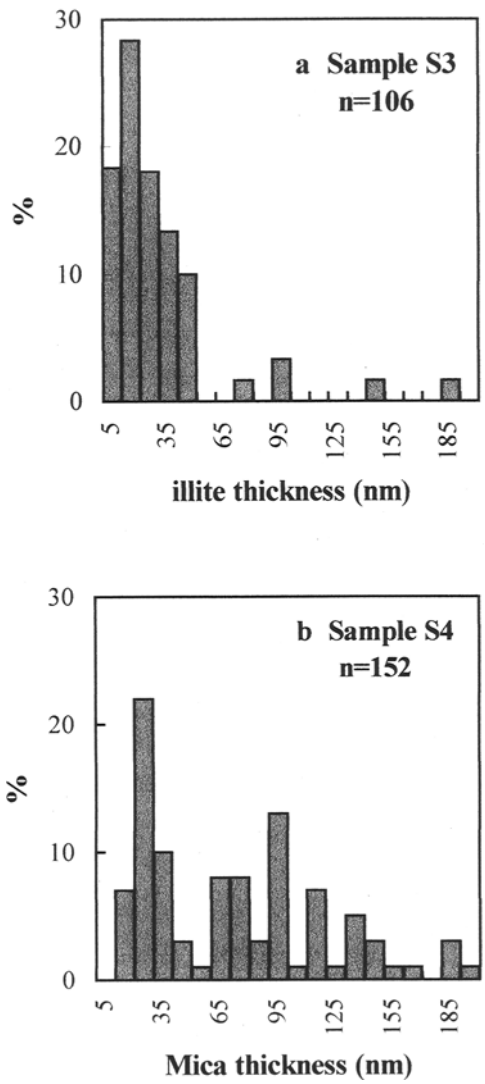


Figure 6. Histograms illustrating the proportion of various thicknesses of illite crystals in sample S3 (a) and mica crystals in sample S4 (b) determined from TEM images.

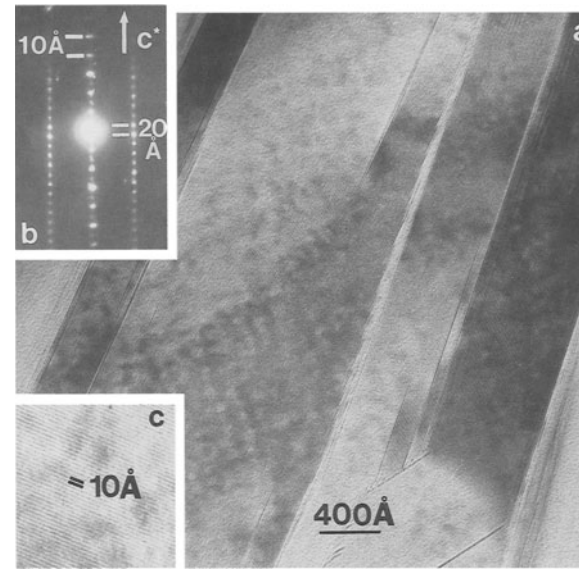


Figure 7. Lattice-fringe images (a, c) and SAED pattern (b) of sample S4, showing muscovite crystals formed by 10-Å fringes with uniform contrast. c) Lattice-fringe image of part of a mica crystal.

these layers were not affected by L.R. White resin. Contrast is relatively uniform throughout a given packet. Illite-packet thicknesses (see Figure 6) are variable, but most crystals are 10–20 layers thick, consistent with a diagenetic grade (Warr and Rice, 1994).

Lateral changes in contrast and spacing of the lattice fringes (Figure 3a) indicate the existence of transitions from I1 I-S (22-Å spacing) to illite layers (10-Å spacing) and from two I1 units to one I3 unit (42-Å spacing). Because such transitions illustrate possible mineralogical transitions not yet complete, all images were carefully examined for their presence. These sequences are very rare in these samples.

SAED patterns of I-S and illite crystals obtained from samples S1, S2, and S3 display high orders of 00*l* reflections with *d*(001) of 10 Å (Figures 3, 4, and 5). Diffuseness normal and parallel to c^* is common; the diffuseness normal to c^* is caused by small variations in orientation of I-S and illite layers or packets whereas that parallel to c^* is caused by mixed layering. Non-00*l* reflections are ill-defined, non-periodic along c^*, and diffuse parallel to c^*, indicating that stacking is partially random. Such SAED patterns have commonly been labeled as being diagnostic of $1M_d$ polytypism. Non-00*l* reflections of SAED patterns of illite from sample S3 (Figure 5d) show minor diffuseness compared to SAED patterns of domains with larger amounts of smectite, as consistent with higher degree of order.

In addition to the basal fringes, some images show 4.5-Å cross fringes formed by imaging *hkl* rows of reflections (Figures 3 and 4). The latter fringes imply that adjacent layers are not turbostratically stacked but they are coherently related by rotations of multiples of ~60°, or semi-coherently related (Guthrie and Reynolds, 1998). Where such cross-fringes do not exist, imaging conditions may not be appropriate for observation and no conclusion regarding stacking can be made. In general, however, layer sequences are disordered but possibly with local ordering over several interlayers.

TEM data for sample S4

Lattice-fringe images of fine-grained matrix phyllosilicates of sample S4 (Figure 7) show packets of well-crystallized mica. Lattice fringes are straight, have uniform contrast, and are continuous over hundreds of angstroms. SAED patterns show reflections

https://doi.org/10.1346/CCMN.2000.0480308 Published online by Cambridge University Press

Table 2. Compositions of the I-S phases of samples S1, S2, and S3 and mica crystals of sample S4 as determined by AEM data. Analyses have been normalized to 22 negative charges. n = number of analyses, Int. Ch. = Interlayer Charge (ΣK + Na + 2Ca), Σoct = sum of octahedral cations.

	S1 n = 12		S2 n = 10		S3 n = 21		S4 n = 13	
	average	range	average	range	average	range	average	range
Si	3.25	3.10–3.51	3.15	3.01–3.30	3.17	3.02–3.31	3.12	3.06–3.19
^{IV}Al	0.75	0.49–0.90	0.85	0.70–0.99	0.83	0.69–0.98	0.88	0.81–0.94
^{VI}Al	1.86	1.71–1.98	1.84	1.71–1.94	1.83	1.60–1.93	1.70	1.63–1.86
Mg	0.16	0.11–0.28	0.17	0.00–0.26	0.18	0.11–0.28	0.29	0.22–0.40
Fe	0.13	0.04–0.22	0.14	0.05–0.27	0.12	0.05–0.42	0.14	0.08–0.25
Σoct	2.15	2.05–2.19	2.15	2.06–2.26	2.13	2.04–2.26	2.13	2.08–2.21
K	0.42	0.18–0.64	0.59	0.39–0.91	0.70	0.53–0.84	0.83	0.49–1.04
Na	0.11	0.00–0.20	0.07	0.00–0.17	0.03	0.00–0.10	0.07	0.00–0.16
Ca	0.03	0.00–0.06	0.02	0.00–0.06	0.02	0.00–0.07	0.00	0.00–0.04
Int. Ch.	0.59	0.34–0.73	0.70	0.39–0.95	0.77	0.63–0.84	0.90	0.63–1.08

with little diffuseness, periodic non-00*l* reflections with 20-Å periodicity corresponding to a two-layer polytype, probably $2M_1$. Analytical electron microscopy (AEM) data (Table 2) show that the micas are K-rich, with high interlayer charge and Si ~ 3.1 per formula unit (p.f.u.), approaching ideal muscovite. They are identified as a mica rather than illite, because illite is characteristically a $1M_d$ polytype with a smaller net layer charge, typically near 0.75, and larger ^{IV}Al content.

TEM images show a broad variation in mica crystal size (thickness) as shown in Figure 6b. Similar mica thicknesses in anchizonal samples were reported by Arkai *et al.* (1996). Despite these variations, mica crystals with 20–30 layers are common. From XRD data, the IC value (CIS scale) is 0.30 °2θ, consistent with a crystal size of 45 nm obtained with the Scherrer equation (Merriman *et al.,* 1990). This value is consistent with anchizonal grade (Warr and Rice, 1994).

AEM analyses

AEM analyses of I-S of samples S1, S2, and S3 and mica crystals of sample S4, normalized on the basis of 22 negative charges (Peacor, 1992) are reported in Table 2. This procedure disregards the possibility of low alkali values caused by diffusion during analysis, but it is not based on the assumption of an ideal dioctahedral structure as is the case for normalizing to a sum of six octahedral and tetrahedral cations. Normalization to 22 negative charges showed a range from 2.13 (samples S3 and S4) to 2.15 (samples S1 and S2) in octahedral occupancy, verifying that octahedral occupancy is nearly ideal, and that the two calculations schemes yield similar formulae.

The total interlayer cation charge Σ(K + Na + 2Ca) increases from 0.59 to 0.90 for samples S1 through S4, as consistent with an increase in the proportion of illite-like layers with increasing grade. Neglecting any iron that is ferric, the formulae for samples S1, S2, and S3 are similar, showing only a small increase in interlayer-cation charge with an increase in the proportion of illite layers. The formula for illite-rich material of sample S4 approaches ideal muscovite. The formulae for the four samples are alike in their ^{VI}Al, Mg, and Fe contents. Although the Fe + Mg content, a measure of the phengite component, varies only from 0.29 (S1) to 0.43 (S4), it is greatest in the highest grade sample.

DISCUSSION

Comparison of XRD and high-resolution (HR) TEM results

XRD data suggest that illitic material of the <2-μm size fractions of samples S1, S2, and S3 consists mainly of discrete illite and minor I-S, whereas this size fraction in sample S4 is comprised of muscovite. TEM data, in contrast, show that the clay minerals in the fine-grained matrices of samples S1 through S4, which represent the authigenic/metamorphic component, are composed of a variety of sequences of illite- and smectite-like layers having a variety of I-values. A given packet may have a dominant layer sequence, but changes in the ordering scheme within an individual packet are common. The values in Table 1 show, however, that the average I-value increases with grade. The distribution of I-values for a given sample shows no preference for odd- or even-numbered values, having an approximately Gaussian form centered on the average value. Sample S3 also contains separate packets with very few smectite-like interlayers, the distribution of I-values being bimodal. We label such material as illite, although it may be described as smectite-poor interstratified I-S.

The clay minerals of the matrix of sample S4 are different from those of sample S3. Packets are larger and contain no smectite-like interlayers. Layer terminations are rarely observed, SAED patterns are consistent with a well-ordered $2M_1$ polytype, and the composition is near muscovite. Although the clay minerals of samples S1 through S4 exhibit features of increas-

https://doi.org/10.1346/CCMN.2000.0480308 Published online by Cambridge University Press

ing grade, samples S1 through S3 imply only small increments of change, whereas sample S4 is consistent with a much larger increment of grade from sample S3 to sample S4. SEM images show also that samples S1 through S3 have a texture typical of clastic sedimentary rocks, whereas S4 is typical of a very low-grade metamorphic rock with weak rock cleavage.

Both XRD and TEM data imply a prograde trend from samples S1 to S4. However, XRD data for samples S1 through S3 imply discrete illite and interstratified I-S. Samples S1 and S2 contain no authigenic illite; the data therefore imply that the <2-μm size fraction contains much detrital mica. For samples S1 and S2, the 10-Å peaks of XRD patterns correspond largely to detrital mica, whereas that for sample S3 has components from detrital mica and authigenic illite. In addition, the XRD data give no direct indication of the specific nature of the I-S interlayering, whereas TEM data show a clearly defined prograde trend in interstratification representative of short-range ordering. XRD is an especially powerful method for the rapid and easy measurement of prograde trends. XRD data, however, integrate over a complex, heterogeneous assemblage of interstratified grains, each packet being partially disordered, rather than representing a collection of grains, each of which is identical; thus, XRD data are a measure of long-range ordering. The data on distribution of I-values described above suggest how such data may be modeled with greater accuracy.

Coherent versus turbostratic layer stacking

The samples contain grains showing a mixture of stacking characteristics ranging from turbostratic to semi-coherent to coherent. The presence of 4.5-Å cross-fringes continuous across a number of 001 fringes in HRTEM images shows that layer stacking was not entirely turbostratic on the scale observable with HRTEM. Whether coherently related (Peacor, 1998) or semicoherent with maximum mis-registry of 10–15° (Guthrie and Reynolds, 1998), layers which display cross-fringes must be stacked with a degree of order. Regions of coherent (or semi-coherent) stacking tend to extend over several layers, commonly encompassing several fundamental particles as defined by Nadeau *et al.* (1984a, 1984b, 1984c); that is, cross-fringes extend across smectite-like interlayers. This is inconsistent with the concept of fundamental particles, because fundamental particles are discrete and require turbostratic stacking at smectite-like interlayers.

However, cross-fringes were only rarely observed. Although the common non-observance of cross-fringes does not prove the existence of turbostratic stacking for an individual particle, non-observance of cross fringes is consistent with turbostratic stacking, which is generally assumed to be dominant in smectite and I-S. Also, the stacking sequence of all authigenic clays in samples S1 through S3 does have a considerable turbostratic component, as indicated in part by the coexistence of 0*kl* and *h*0*l* reflections in SAED patterns which include c^*. SAED patterns with 0*kl* rows have diffuse, non-periodic, weak 0*kl* reflections ($k \neq 3n$), as typical of $1M_d$ polytypism, and it is those reflections which are the source of cross-fringes, and which demonstrate local coherency. The SAED patterns and lattice-fringe images thus define stacking sequences in I-S as having a complex combination of both turbostratic and coherent to semi-coherent stacking, the proportion of coherent interfaces assumedly increasing with increasing proportion of illite-like layers (Dong and Peacor, 1996; Peacor, 1998). That is, such layer sequences do not consist entirely of separate, stacked layers (*i.e.,* fundamental particles), but at least in part are comprised of three-dimensionally periodic arrays.

Transition mechanisms

Although many mechanisms were proposed for illitization, two mechanisms represent extremes: layer-by-layer replacement and massive dissolution-crystallization. Altaner and Ylagan (1997) reviewed evidence for both mechanisms, and although they indicated that processes involving a fluid phase can not be rejected, they consider the layer-by-layer replacement to occur in the solid state, *sensu strictu.* They concluded that fluid/rock ratio and permeability influence the reaction mechanism, *e.g.,* bentonites commonly have low permeability and the resulting low fluid/rock ratio inhibits large-scale dissolution and crystallization, whereas high permeability of hydrothermal systems and sandstones favors a greater degree of dissolution and recrystallization. Both dissolution/crystallization and solid-state transformation can occur in shales.

Layer-by-layer replacement of one phyllosilicate by another has been documented by TEM studies. Giorgetti *et al.* (pers. comm.) noted that the term "solid state reaction" implies only that the reactant and product structures are closely related. They noted that a fluid at the one-dimensional reaction interface is essential to transport components, as documented, *e.g.,* in the replacement of biotite by kaolinite (Ahn and Peacor, 1987), and that time required for true solid-state diffusion to and from the reaction interface is tens of orders of magnitude too slow for the reaction rates.

The increase in the proportion of illite-like layers with increase in burial depth in this study is the first example of an apparently continuous sequence of changes studied by TEM. The layer-by-layer replacement mechanism requires such a systematic sequence. However, one problem with this mechanism is the inability of illite-rich sequences to be derived from, for example, I1 I-S. Replacement of smectite-like layers can not produce, *e.g.,* I2 I-S; *i.e.,* replacement of one S layer of an . . . ISISIS . . . sequence produces a se-

https://doi.org/10.1346/CCMN.2000.0480308 Published online by Cambridge University Press

quence with an I3 unit, as in . . . ISIIIS . . . The observations of this study show that each sample is composed of packets with a range of I-values, however. Replacement of smectite-like layers in a lower-grade sample is thus capable of generating the I-values present in a higher-grade sample. Layer-by-layer transformations also require the presence of lateral transitions. TEM observations show that replacement may start in a single layer at a grain boundary and the linear interface then advances across the entire layer. The transitions observed in sample S1 from I1 I-S to illite layers and from I1 to I3 units thus support a layer-by-layer mechanism.

On the other hand, layer transitions were only rarely observed despite careful observations of many images. Observation of apparently continuous changes in I-values with increase in grade is a necessary condition for the layer-by-layer mechanism; it is not sufficient to prove such a relation, however. The same layer sequences may be generated where the clay minerals are simultaneously neocrystallized at all depths, as in Salton Sea sediments (Yau *et al.,* 1984) or as postulated for Gulf Coast diagenesis by Morton (1985) and Ohr *et al.* (1991).

The TEM observations are therefore highly suggestive of, but do not require, a layer-by-layer transition for samples S1 through S3. Whether such a transition occurs, the continuous sequence in I-values is unique, and in sharp contrast to the discontinuous sequence of phases as observed by Dong *et al.* (1997). They described TEM observations of shales from the Gulf Coast and elsewhere in which only smectite, (R = 1) I-S, and illite occurred. Such differences are expected from thermodynamic considerations, however, because smectite and I-S are metastable, transitions therefore occur according to the Ostwald step rule, and intermediate phases are determined by rates of reaction (Essene and Peacor, 1995). Thus, a wide variety of textures is possible, and disagreement about illite-smectite transition mechanisms may in part reflect the wide variety of textures and phases possible in many rock types.

Although the series of I-S phases in samples S1 through S3 appears to be continuous, the change from $1M_d$ illite of sample S3 to the $2M_1$ muscovite of S4 is clearly discontinuous. The discontinuous character of the bimodal distribution of clays in sample S3 occurs also. The structural reorganization required of the illite to muscovite transition, the increase in crystallite size with a lack of cores of lower-grade clays, and the change in orientation resulting in rock cleavage, are consistent with a dissolution-crystallization origin.

Chemical compositions of the I-S phases

Several authors (Ahn and Peacor, 1986; Jiang *et al.,* 1990; Vali *et al.,* 1994; Jakobsen *et al.,* 1995) suggested that (R = 1) I-S does not consist simply of alternating illite-like and smectite-like layers. The ordered interstratified structure is believed to consist of 2:1 layer units having Al-Si distributions that are symmetrical across interlayers, not octahedral sheets (Brown and Weir, 1963; Barron *et al.,* 1985; Ahn and Peacor, 1986; Nadeau and Bain, 1986; Altaner *et al.,* 1988; Dong *et al.,* 1997). Alternate interlayers may thus be bounded by two high-charge (high Al) and two low-charge (high Si) tetrahedral sheets, respectively. Jiang *et al.* (1990) emphasized that rectorite has a composition similar to that of illite (0.7–0.8K per 11 oxygens) and not a weighted average of those of smectite and illite, and this is observed in the I-S compositions of our samples. This observation is consistent also with Dong *et al.* (1997) and Ransom and Helgeson (1993). In contrast, Środoń *et al.* (1986) found that the content of fixed-K per illite layer is not constant, but ranges continuously from 0.55 (per 11 oxygens) for illite layers in randomly interstratified (R = 0) I-S to 1.0 for illite layers formed in ordered (R > 0) I-S. However, their compositions were from bulk chemical analyses, and there is no direct comparison with our AEM analyses of specific layer sequences.

Chemical compositions of the I-S of samples of this study, normalized on the basis of 22 negative charges, have interlayer charges varying from 0.59 (S1) to 0.77 (S3), to 0.90 for muscovite-like material (S4). The compositions of I-S therefore reflect increasing occupancy of interlayer sites in response to increasing net negative charge with increasing proportion of illite-like layers, although the changes are small. The average formulae of samples S1, S2, and S3 are strikingly similar despite the significant change in ratio of smectite- to illite-like layers. The change in net negative charge is derived from small changes in ^{IV}Al, which increases from 0.75 in sample S1 to 0.83 in sample S3, also consistent with the increasing proportion of illite-like layers. The interlayer K content shows the largest variation, increasing from 0.42 to 0.70 p.f.u., compensated in part by a small decrease in Na content. These data support the concept that I-S with relative proportions of smectite-like and illite-like layers intermediate to (R = 1) I-S and illite differ only slightly in composition as a result of unique Al-Si distributions relative to smectite and muscovite. The small changes in average composition are significant as measures of relative proportions of illite-like and smectite-like layers in I-S.

The increase in interlayer charge from S3 (0.77) to S4 (0.90) is derived almost entirely from an increase in octahedral Fe + Mg (0.30–0.43), a measure of the phengite component, rather than primarily in an increase in ^{IV}Al (0.83–0.88). The composition approaches, but does not reach, the mature compositions of phengitic muscovite typical of higher grade rocks.

https://doi.org/10.1346/CCMN.2000.0480308 Published online by Cambridge University Press

$1M_d$ to $1M$ to $2M_1$ polytype transitions

Numerous XRD studies (*e.g.*, Maxwell and Hower, 1967; Frey, 1987; Yang and Hesse, 1991) documented prograde changes in polytypism from $1M_d$ to $1M$ and $2M_1$ in white micas. Because XRD patterns showed discrete illite in samples studied here, two methods were used to determine the relative proportion of polytypes. These data indicated an increase in the $2M_1/(2M_1 + 1M + 1M_d)$ ratio from sample S1 (0.2) to S4 (1). The TEM data show, however, that there is substantial $2M_1$ detrital mica in all samples. The data imply that the illite in samples S1 and S2 is detrital, substantial authigenic illite coexists with detrital illite in sample S3, and $2M_1$ authigenic illite occurs in sample S4. Furthermore, no $1M$ illite was observed in any sample. All I-S and authigenic illite in samples S1 through S3 show $1M_d$ polytype as described by Grubb *et al.* (1991) and Dong and Peacor (1996). The sequential change in polytypism implied by XRD data is therefore not a measure of the relative proportion of the $2M_1$ polytype of authigenic illite relative to $1M$, except for sample S4. Rather, the XRD patterns originate from integration of complex, heterogeneous diffraction patterns from individual packets with non-periodic, diffuse, and ill-defined non-00*l* reflections. Caution should be exercised in interpretations of relative proportions of polytypes by XRD in samples from other localities, as the $1M$ polytype is extremely rare, $1M_d$ as originally defined has never been observed, and SAED patterns have characteristics which have yet to be correlated with features of XRD patterns (Dong and Peacor, 1996).

ACKNOWLEDGMENTS

The authors thank D. Yates, G. Guthrie, S. Guggenheim, and P. Heaney for helpful suggestions for improving the manuscript. The authors are grateful to L.-S. Kao for help in sample preparation. This work supported by National Science Foundation grants EAR 9418108 and 9814391 to D.R. Peacor. B. Bauluz is grateful to M.M. Abad for training in use of the TEM.

REFERENCES

Ahn, J.H. and Peacor, D.R. (1986) Transmission and analytical electron microscopy of the smectite-to-illite transition. *Clays and Clay Minerals,* **34,** 165–179.

Ahn, J.-H. and Peacor, D.R. (1987) Kaolinitizacion of biotite: TEM data and implications for an alteration mechanism. *American Mineralogist,* **72,** 353–356.

Ahn, J.H. and Peacor, D.R. (1989) Illite/smectite from Gulf Coast shales: A reappraisal of transmission microscope images. *Clays and Clay Minerals,* **37,** 542–546.

Altaner, S.P. and Ylagan, R.F. (1997) Comparison of structural models of mixed-layer illite/smectite and reaction mechanisms of smectite illitization. *Clays and Clay Minerals,* **45,** 517–533.

Altaner, S.P., Whitney, G., Aronson, J.L., and Hower, J. (1984) A model for K-bentonite formation, evidence from zoned K-bentonites in the disturbed belt, Montana. *Geology,* **12,** 412–415.

Altaner, S.P., Weiss, C.A., Jr., and Krikpatrick, R.J. (1988) Evidence from ^{29}Si NMR for the structure of mixed-layer illite/smectite clay minerals. *Nature,* **331,** 699–702.

Arkai, P., Merriman, R.J., Roberts, B., Peacor, D.R., and Toth, M. (1996) Crystallinity, crystallite size and lattice strain of illite-muscovite and chlorite: Comparison of XRD and TEM data for diagenetic to epizonal pelites. *European Journal of Mineralogy,* **8,** 1119–1137.

Barron, P.F., Slade, P., and Frost, R.L. (1985) Ordering of aluminum in tetrahedral sites in mixed-layer 2:1 phyllosilicates by solid-state high-resolution NMR. *Journal of Physical Chemistry,* **89,** 3880–3885.

Bauluz, B. (1997) Caracterización mineralógica y geoquímica de materiales detríticos precámbricos y paleozoicos de las Cadenas Ibéricas: Evolución post-sedimentaria. Ph.D. thesis, University of Zaragoza, Spain, 341 pp.

Bauluz, B., Mayayo, M.J., Fernandez-Nieto, C., and Gonzalez Lopez, J.M. (1995) Mineralogy and geochemistry of Devonian detrital rocks from the Iberian Range (Spain). *Clay Minerals,* **30,** 381–394.

Bauluz, B., Fernandez-Nieto, C., and Gonzalez-Lopez, J.M. (1998) Diagenesis—very low-grade metamorphism of clastic Cambrian and Ordovician sedimentary rocks in the Iberian Range (Spain). *Clay Minerals,* **33,** 373–394.

Brown, G. and Weir, A.H. (1963) The identity of rectorite and allevardite. In *Proceedings of International Clay Conference Stockholm, Sweden, Volume 1,* Th. Rosenquest und P. Graff-Petterson, eds., Pergamon Press, Oxford, 27–35.

Brusewitz, A. (1986) Chemical and physical properties of Paleozoic potassium bentonites from Kinnekulle, Sweden. *Clays and Clay Minerals,* **34,** 442–454.

Buatier, M., Peacor, D.R., and O'Neil, J.R. (1992) Smectite-illite transition in Barbados accretionary wedge sediments: TEM and AEM evidence for dissolution/crystallization at low temperature. *Clays and Clay Minerals,* **40,** 65–80.

Caillere, S., Henin, S., and Rautureau, M. (1982) *Mineralogie des Argiles. II. Classification et Nomenclature.* Masson, Paris, 45–87.

Dong, H. and Peacor, D.R. (1996) TEM observations of coherent stacking relations in smectite, I/S and illite of shales: Evidence for McEwan crystallites and dominance of $2M_1$ polytypism. *Clays and Clay Minerals,* **44,** 257–275.

Dong, H., Peacor, D.R., and Freed, R.L. (1997) Phase relations among smectite, R1 illite-smectite, and illite. *American Mineralogist,* **82,** 379–391.

Essene, E.J. and Peacor, D.R. (1995) Clay mineral thermometry—A critical perspective. *Clays and Clay Minerals,* **43,** 540–553.

Freed, R.L. and Peacor, D.R. (1992) Diagenesis and the formation of authigenic illite-rich I/S crystals in Gulf Coast shales: TEM study of clay separates. *Journal of Sedimentary Petrology,* **62,** 220–234.

Frey, M. (1987) Very low-grade metamorphism of clastic sedimentary rocks. In *Low Temperature Metamorphism,* M. Frey, ed., Blackie, Glasgow, 9–58.

Grubb, S.M.B., Peacor, D.R., and Jiang, W-T. (1991) Transmission electron microscope observations of illite polytypism. *Clays and Clay Minerals,* **39,** 540–550.

Guthrie, G.D. and Reynolds, R.C., Jr. (1998) A coherent TEM- and XRD-description of mixed-layer illite/smectite. *Canadian Mineralogist,* **36,** 1421–1434.

Guthrie, G.D. and Veblen, D.R. (1989a) High-resolution transmission electron microscopy of mixed-layer illite/smectite: Computer simulation. *Clays and Clay Minerals,* **37,** 1–11.

Guthrie, G.D. and Veblen, D.R. (1989b) High-resolution transmission electron microscopy applied to clay minerals. In *Spectroscopic Characterization of Minerals and Their Surfaces,* L.M. Coyne, S.W.S. McKeever, and D.F. Blake,

https://doi.org/10.1346/CCMN.2000.0480308 Published online by Cambridge University Press

eds., Symposia Series 415, American Chemical Society, Washington, D.C., 75–93.

Guthrie, G.D. and Veblen, D.R. (1990) Interpreting one-dimensional high-resolution transmission electron micrographs of sheet silicates by computer simulation. *American Mineralogist,* **75,** 276–288.

Horton, D.G. (1985) Mixed-layer illite/smectite as a paleotemperature indicator in the Amethyst vein system, Creede district, Colorado, USA *Contributions to Mineralogy and Petrology,* **91,** 171–179.

Hower, J., Eslinger, E.V., Hower, M.E., and Perry, E.A. (1976) Mechanism of burial metamorphism of argillaceous sediments: Mineralogical and chemical evidence. *Geological Society of America Bulletin,* **87,** 725–737.

Jadgozinski, H. (1949) Eindimensionale fehlordnung in kristallen und ihr einfluss auf die Rontgeninterferenzen. I. Berechnung des fehlordnungsgrades au der Rontgenintensitaten. *Acta Crystallographica,* **2,** 201–207.

Jakobsen, H.J., Nielsen, N.C., and Lindgreen, H. (1995) Sequences of charged sheets in rectorite. *American Mineralogist,* **80,** 247–252.

Jiang, W-T. and Peacor, D.R. (1993) Formation and modification of metastable intermediate sodium potassium mica, paragonite, and muscovite in hydrothermally altered metabasites from northern Wales. *American Mineralogist,* **78,** 782–793.

Jiang, W-T., Peacor, D.R., Merriman, R.J., and Roberts, B. (1990) Transmission and analytical electron microscopic study of mixed-layer illite/smectite formed as an apparent replacement product of diagenetic illite. *Clays and Clay Minerals,* **38,** 449–469.

Kim, J.W., Peacor, D.R., Tessier, D., and Elsass, F. (1995) A technique for maintaining texture and permanent expansion of smectite interlayers for TEM observations. *Clays and Clay Minerals,* **43,** 51–57.

Kisch, H.J. (1991) Development of slaty cleavage and degree of very-low grade metamorphism: A review. *Journal of Metamorphic Geology,* **9,** 735–750.

Kubler, B. (1967) Anchimetamorphisme et schistosite. *Bulletin du Centre de Recherches de Pau,* **1,** 259–278.

Lee, J.H.K., Peacor, D.R., Lewis, D.D., and Wintsch, R.P. (1985) Chlorite-illite/muscovite interlayered and interstratified crystals: A TEM/STEM study. *Contributions to Mineralogy and Petrology,* **88,** 372–385.

Maxwell, D.T. and Hower, J. (1967) High-grade diagenesis and low-grade metamorphism of illite in the precambrian belts series. *The American Mineralogist,* **52,** 843–857.

Merriman, R.J., Roberts, B., and Peacor, D.R. (1990) A transmission electron microscope study of white mica crystallite size distribution in a mudstone to slate transitional sequence, North Wales, UK. *Contributions to Mineralogy and Petrology,* **106,** 27–40.

Morton, J.P. (1985) Rb-Sr evidence for punctuated illite/smectite diagenesis in the Oligocene Frio Formation, Texas Gulf Coast. *Geological Society of America Bulletin,* **96,** 114–122.

Nadeau, P.H. and Bain, D.C. (1986) Composition of some smectites and diagenetic illitic clays and implications for their origin. *Clays and Clay Minerals,* **34,** 455–464.

Nadeau, P.H., Tait, J.M., McHardy, W.J., and Wilson, M.J. (1984a) Interstratified XRD characteristics of physical mixtures of elementary clay particles. *Clay Minerals,* **19,** 67–76.

Nadeau, P.H., Wilson, M.J., McHardy, W.J., and Tait, J.M. (1984b) Interstratified clays as fundamental particles. *Science,* **225,** 923–925.

Nadeau, P.H., Wilson, M.J., McHardy, W.J., and Tait, J.M. (1984c) Interparticle diffraction: A new concept for interstratified clays. *Clay Minerals,* **19,** 757–769.

Nadeau, P.H., Wilson, M.J., McHardy, W.J., and Tait, J.M. (1985) The conversion of smectite to illite during diagenesis. Evidence from some illitic clays from bentonites and sandstones. *Mineralogical Magazine,* **49,** 393–400.

Ohr, M., Halliday, A.N., and Peacor, D.R. (1991) Sr and Nd isotopic evidence for punctuated clay diagenesis, Texas Gulf Coast. *Earth and Planetary Science Letters,* **105,** 110–126.

Peacor, D.R. (1992) Analytical electron microscopy: X-ray analysis. In *Analytical Electron Microscopy: X-ray Analysis, Reviews in Mineralogy, Volume 27,* P.R. Buseck, ed., Mineralogical Society of America, Washington, D.C., 113–140.

Peacor, D.R. (1998) Implications of TEM data for the concept of fundamental particles. *Canadian Mineralogist,* **36,** 1397–1408.

Ransom, B. and Heldeson, H.C. (1993) Compositional end members and thermodynamic components of illite and dioctahedral aluminous smectite solid solutions. *Clays and Clay Minerals,* **41,** 537–550.

Środoń, J. and Eberl, D.D. (1984) Illite. In *Micas, Reviews in Mineralogy, Volume 13,* P.H. Ribbe, ed., Mineralogical Society of America, Washington, D.C., 495–544.

Środoń, J., Morgon, D.J., Eslinger, E.V., Eberl, D.D., and Karlinger, M.R. (1986) Chemistry of illite/smectite and end member illite. *Clays and Clay Minerals,* **34,** 368–378.

Vali, H., Hesse, R., and Martin, R.F. (1994) A TEM-based definition of 2:1 layer silicates and their interstratified constituents. *American Mineralogist,* **79,** 644–653.

Veblen, D.R., Guthrie, G.D., Jr., Livi, K.J.T., and Reynolds, R.C., Jr. (1990) High-resolution transmission electron microscopy and electron diffraction of mixed-layer illite/smectite: Experimental results. *Clays and Clay Minerals,* **38,** 1–13.

Warr, L.N. and Rice, A.H.N. (1994) Interlaboratory standardization and calibration of clay mineral crystallinity size data. *Journal of Metamorphic Geology,* **12,** 141–152.

Yang, C. and Hesse, R. (1991) Clay minerals as indicators of diagenetic and anchimetamorphic grade in an overthrust belt, external domain of southern Canadian Appalachians. *Clay Minerals,* **26,** 211–231.

Yau, Y.C., Anovitz, L.M., Essene, E.J., and Peacor, D.R. (1984) Phlogopite-chlorite reaction mechanisms and physical conditions during retrograde reactions in the Marble Formation, Franklin, New Jersey. *Contributions to Mineralogy and Petrology,* **88,** 299–306.

E-mail of corresponding author: bauluz@posta.unizar.es

(Received 3 July 1999; accepted 22 February 2000; Ms. 358; A.E. Peter J. Heaney)

https://doi.org/10.1346/CCMN.2000.0480308 Published online by Cambridge University Press